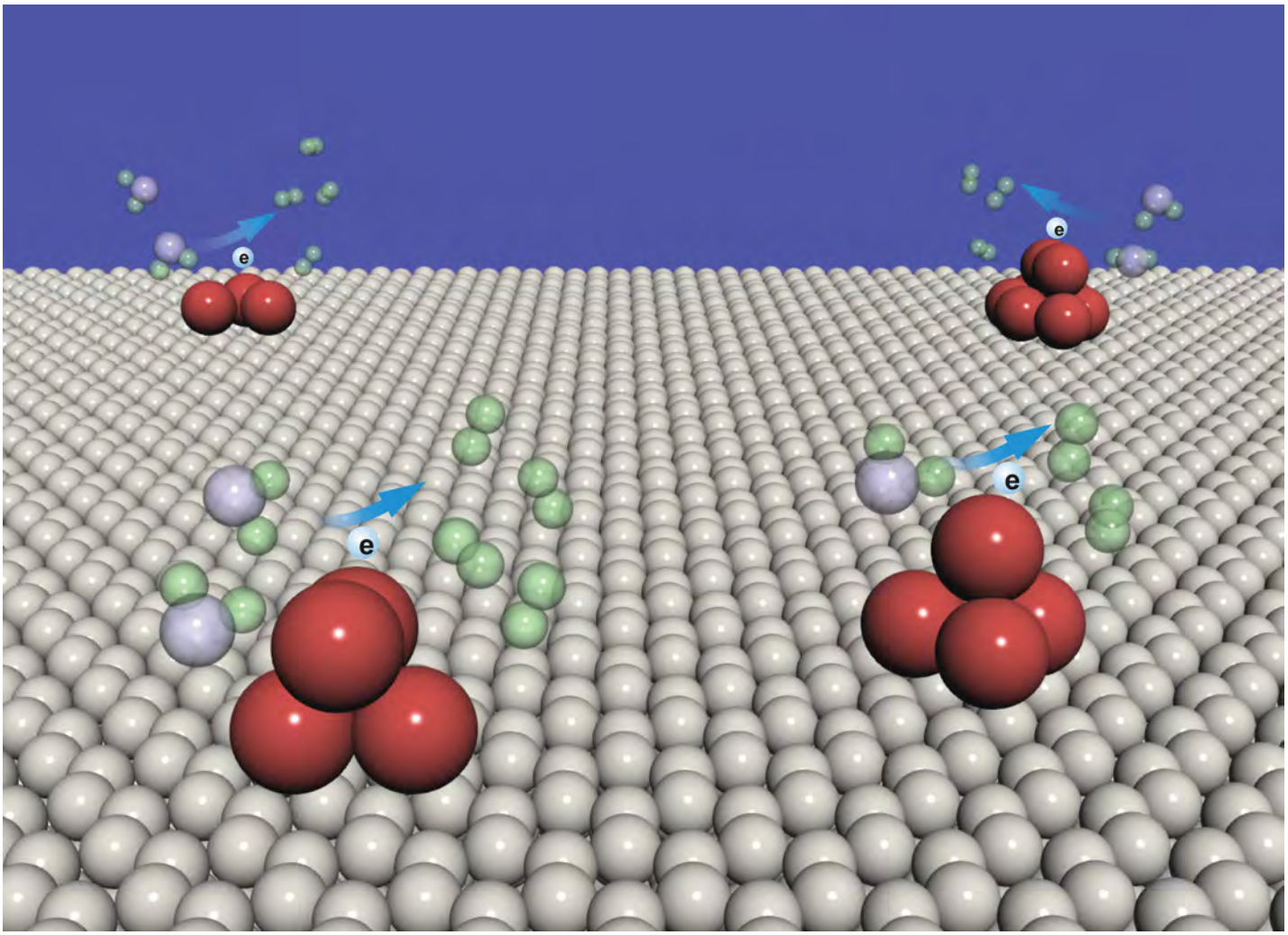

Showcasing the study on electrochemical activation of carbon-based cathodes for hydrogen evolution reaction by the group of Dr. Johnny C. Ho at Department of Physics and Materials Science, City University of Hong Kong.

Title: Insight into the electrochemical activation of carbon-based cathodes for hydrogen evolution reaction

An efficient activation of carbon materials was achieved only when platinum was used as the counter electrode and, simultaneously, Pt transfer from the anode to the cathode was observed, indicating that the improved hydrogen evolution reaction performance was mainly caused by the Pt transfer, rather than the activation of carbon materials themselves as has been suggested in previous publications.

As featured in:

See Sai Tak Chu, Johnny C. Ho *et al.*, *J. Mater. Chem. A*, 2015, **3**, 13080.

ROYAL SOCIETY OF CHEMISTRY

www.rsc.org/MaterialsA

Registered charity number: 207890

Journal of Materials Chemistry A

PAPER

Cite this: J. Mater. Chem. A, 2015, 3, 13080

Insight into the electrochemical activation of carbon-based cathodes for hydrogen evolution reaction†

Guofa Dong,‡[ab] Ming Fang,‡[ab] Hongtao Wang,[c] Senpo Yip,[ab] Ho-Yuen Cheung,[d] Fengyun Wang,[e] Chun-Yuen Wong,[d] Sai Tak Chu*[a] and Johnny C. Ho*[ab]

Received 8th April 2015
Accepted 6th May 2015

DOI: 10.1039/c5ta02551f

www.rsc.org/MaterialsA

Recently, carbon nanomaterials with outstanding electrocatalytic performance for the hydrogen evolution reaction (HER) after electrochemical activation have been reported; however, the exact activation mechanism is still under extensive debate. In this study, to better understand the activation, graphite rods and carbon nanohorns, two typical carbon materials in different scales, were electrochemically activated and their catalytic performances in HER were systematically studied, which showed that the HER performance was greatly affected by the counter electrode employed for the activation. An efficient activation was achieved when a platinum wire was used as the counter electrode; simultaneously, Pt transfer from the anode to the cathode was also observed. These results suggest that the improved HER performance was mainly caused by the Pt transfer, rather than the activation of the carbon materials themselves. More importantly, our study implied that the Pt dissolution, although widely ignored, should be taken into consideration during electrochemical tests when Pt metal is utilized as the counter electrode.

1. Introduction

Due to its superior efficiency, zero pollution and good recyclability, hydrogen has been considered as one of the most promising alternative fuels for tackling the problems of energy crisis, as well as environmental pollution in the future.[1,2] In general, electrolysis of water, an important method for hydrogen production, has been employed in various industrial processing sectors for decades and has recently attracted more and more interest for energy applications. However, owing to the obstacle of overpotential, the required potential in water electrolysis is always much higher than the standard value, which inevitably leads to a huge waste of power.[3,4] In order to improve the efficiency of water electrolysis, noble metal catalysts, such as Pt, Pd, Ru, or their alloys, are often adopted and integrated into the electrodes to lower the overpotential because of their excellent electrocatalytic performance on the hydrogen evolution reaction (HER).[5,6] However, these noble metals are not only expensive, but also scarce with limited reserves on the earth; as a result, all these noble catalysts are far from sustainable in the future development of hydrogen evolution. In this regard, developing novel and low-cost catalysts with high catalytic performance for HER is an imperative task in the research of electrochemical water splitting.[7,8]

In the past few years, many promising non-noble electrocatalysts, including transition metal sulfides, selenides, borides, carbides, nitrides and phosphides, have been extensively exploited for HER.[5,9,10] Nevertheless, achieving efficient catalysts with high activity and good stability for HER is still a big challenge. Until recently, carbon nanomaterials, such as carbon nanotubes and fullerenol, were reported with outstanding catalytic performance in HER after electrochemical activation.[11–13] In particular, the activated single-walled carbon nanotube film has exhibited remarkable electrocatalytic performance, almost as good as that of platinum in HER.[13] Some researchers also proposed the mechanism for this activation and attributed these performance improvements to the increase in the number of oxygen functionalities, which were considered as the active sites for HER, or the "adjacent Tafel" mechanism,[11–13] but the exact mechanism is still

[a]Department of Physics and Materials Science, City University of Hong Kong, 83 Tat Chee Avenue, Kowloon Tong, Kowloon, Hong Kong. E-mail: johnnyho@cityu.edu.hk; saitchu@cityu.edu.hk

[b]Shenzhen Research Institute, City University of Hong Kong, Shenzhen, People's Republic of China

[c]State Key Laboratory of Silicon Materials, Key Laboratory of Advanced Materials and Applications for Batteries of Zhejiang Province, School of Materials Science and Engineering, Zhejiang University, Hangzhou, People's Republic of China

[d]Department of Biology and Chemistry, City University of Hong Kong, 83 Tat Chee Avenue, Kowloon, Hong Kong

[e]Cultivation Base for State Key Laboratory, Qingdao University, No. 308 Ningxia Road, Qingdao, People's Republic of China

† Electronic supplementary information (ESI) available: Experimental details of Pt/C powder and CNHs, the details about the EDS analysis of Pt wire and graphite rod, additional electrochemical data and TEM image of CHNs. See DOI: 10.1039/c5ta02551f

‡ These authors contributed equally to this work.

unclear. In some previous studies, carbon materials surprisingly gave poor catalytic activity on HER[14] and were often used as structural scaffolds for catalysts.[7,15–17] In this study, in order to obtain a better and clearer understanding of this activation, pure graphite rods were utilized as the working electrode and were electrochemically activated. It was found that the type of counter electrode employed for the activation could fundamentally determine the HER performance of the working electrodes after activation. When a Pt wire was used as the counter electrode, the working electrode could be effectively activated after 13 000 cyclic voltammetry (CV) cycles and yielded extraordinary catalytic performance for HER. However, with a graphite rod as the counter electrode, even increasing the activation to 15 000 CV cycles or after a potentiostatic treatment of 20 000 s at −2.0 V, there was almost no improvement. Further characterization by SEM, TEM and XPS verified that when the counter electrode was a Pt wire, Pt nanoparticles were formed on the working electrode and actually led to the improved electrocatalysis on HER. Carbon nanohorns, as metal-free nano-sized carbon materials,[18,19] were also treated with the same activation procedure and similar results to those on the graphite rods were obtained. All these results imply that the anodic platinum dissolution and subsequent transfer during the potential scan cycles must be responsible for the formation of Pt nanoparticles on the cathode. We hereby suggest that CV cycling is not a valid method for activating carbon materials into efficient HER catalysts, and metal contamination should be taken into consideration during electrochemical tests when Pt is used as the counter electrode.

2. Experimental

2.1 Materials

Isopropyl alcohol (99.7%), sulphuric acid (H_2SO_4, >95%) and Nafion solution (5% in a mixture of lower aliphatic alcohols and water) were purchased from Sigma-Aldrich. All chemicals were used as received without further purification. Pure graphite rods (8 mm in diameter, 99.999% purity trace metals basis) were obtained from Shanghai New Graphite Material CO., LTD. The commercial Pt/C powder (20 wt% Pt on Vulcan XC-72) was purchased from Alfa Aesar. The platinum wire is commercially available and with a purity of 99.99 wt%. Water used throughout the experiments was purified through a Millipore system.

2.2 Fabrication of the working electrode

In order to exclude the interference from metal elements to the greatest extent, highly pure graphite rods were used as the working electrodes or counter electrode. Herein, the working electrodes were fabricated by the following processes. The graphite rods were first cut into a length of ~ 3 cm. Next, the cross sections of the graphite electrodes were polished with SiC abrasive paper (Eagle, 1500 type) and weighing paper and then washed ultrasonically with water twice to get rid of the remaining graphite powder. Finally, the column parts of the working electrode were sealed with water-proof tape and only the smooth cross section was exposed as the reactive interface for the experiment. It is noted that two graphite working electrodes were newly fabricated and used separately for the activations with different counter electrodes.

2.3 Preparation of carbon nanohorns

Carbon nanohorns (CNHs) were prepared by a modified arc discharge method reported in the literature.[19] Typically, two highly pure graphite rods with a diameter of 8 mm reacted under a DC arc-discharge in a water-cooled stainless steel chamber filled with 400 Torr of air as the buffer gas. The discharge current was kept at about 140 A. As the anode was consumed, the distance between the two electrodes was maintained at a constant value of about 1 mm. After the discharge, the chamber was cooled down to room temperature and opened. Then, the soot on the inner and upper wall of the reaction chamber was collected for further use.

2.4 Instrumentation and measurements

Scanning electron microscopy (SEM) images were taken on a Phenom Pro SEM (FEI, US) and a Hitachi SU-70 SEM system (Hitachi, Japan). Transmission electron microscopy (TEM) and HR-TEM images were obtained by a Tecnai G2 F20 S-TWIN (FEI, US) field emission electron microscope and the acceleration voltage was 200 kV. High-angle annular dark-field scanning transmission electron microscopy (HAADF-STEM) and corresponding energy-dispersive X-ray spectroscopy (EDS) mapping analysis were performed on a Titan G2 80-200 TEM/ChemiSTEM (FEI, US) with a spherical aberration corrector. X-ray photoelectron spectra (XPS) were acquired on an ESCALAB 250 XPS system. Before all the measurements, the electrode surfaces were washed with DI water several times and dried at 50 °C in open air. For the TEM observation, a thin surface layer of the electrode was gently scratched off from the working area and ultrasonically dispersed in absolute ethanol. Then, a droplet of the abovementioned dispersion was dropped on the copper micro-grid coated with holey carbon and dried in open air. The purity of Pt wire was determined on an Environmental Scanning Electron Microscope (FEI/Philips XL30 ESEM-FEG) system before electrochemical activation, and the corresponding details are shown in ESI.†

2.5 Electrochemical measurements

A standard electrochemical cell with three electrodes was set up for all the electrochemical activations and electrochemical tests. A Pt wire or a graphite rod was used as the counter electrode and a saturated calomel electrode (SCE) was used as the reference electrode. All electrochemical activations and determinations were performed on a G300 workstation (Gamry Instruments, USA). Herein, for simplicity, we denote the working graphite electrodes as Pt-GE and G-GE, respectively, when the Pt wire or graphite rod was used as the counter electrode for activation. Electrochemical activations were carried out by CV scan in a potential range from −0.56 V to +0.24 V with a scan rate of 50 mV s^{-1}. The electrocatalytic activities towards HER were determined by linear sweep voltammetry (LSV) with a scan rate

of 5 mV s^{-1}. For the purpose of comparison, the catalytic performance of the commercial Pt/C powder (20 wt% Pt on Vulcan XC-72) was also measured under similar conditions by loading it on a glassy carbon working electrode (GCE). The Pt/C powder was loaded by the drop casting method and the details can be found in the ESI.† The catalytic activity of CNH for HER was also determined by the same procedure exploited on Pt/C powder. All the electrochemical activations or examinations were carried out at room temperature in 0.5 M H_2SO_4 solution. For every electrochemical experiment, the cell was first washed with DI water and then rinsed with 0.5 M H_2SO_4 solution before the new electrolyte was added. All the potentials reported in this study were referred to a reversible hydrogen electrode (RHE) by adding a value of (0.242 + 0.059 × pH) V and all the LSV curves were corrected through the iR compensation to eliminate the error from the internal resistance. All the current density values were determined based on the geometric area of the electrode.

3. Results and discussion

3.1 The electrocatalytic activity on HER

As mentioned above, the working graphite rods were activated by continuous potential scan with different counter electrodes. Then, the corresponding LSV curves were recorded in order to investigate their electrocatalytic activity on HER. Fig. 1 demonstrates all the polarization curves measured from different graphite rods. It is clear that before activation, the graphite rods showed a substantial overpotential of more than 500 mV whenever either a Pt wire or a graphite rod was utilized as the counter rod. When a graphite rod was used as the counter electrode, there was no apparent improvement in the HER electrocatalytic activity even after 15 000 CV activation cycles (Fig. 1b). The onset potential for HER was still at about −480 mV and the corresponding current density was just about 0.7 mA cm^{-2}, which indicated that the G-GE failed to be activated. However, when a Pt wire was employed as the counter electrode and after 13 000 CV cycles of activation, the HER overpotential was sharply decreased to 20 mV, while the corresponding current density was still maintained at ~10.4 mA cm^{-2} (Fig. 1a). These values were very close to those determined using the commercial Pt/C. Obviously, the graphite rod was effectively activated after pre-treatment with a Pt wire as the counter electrode. All these results explicitly indicate that the type of counter electrodes exploited for the activation plays a decisive role in the HER activity of the activated working graphite rod.

3.2 Functional details of counter electrodes

Since all electrode reactions are essentially the interfacial processes occurring between the solid surface of the electrode and the adjacent thin layer of the solution, the surface properties of electrodes play a crucial role in these interfacial reactions. Many factors, such as the chemical composition, structure, morphology and electrical properties of the electrode surface, would fundamentally determine the possibility, direction and reactive rate of the electrode reactions; therefore, the working graphite rod was thoroughly examined by SEM, TEM, XPS and EDS mapping in order to further understand the functional details of counter electrodes during the activation process.

Surface morphologies. Fig. 2 depicts all the SEM images of the graphite rod surfaces. As shown in Fig. 2a, it is evident that before any activation, the initial surface of the graphite electrode was very rough and disordered, full of graphite flakes or particles, although it looked very flat and smooth to the naked

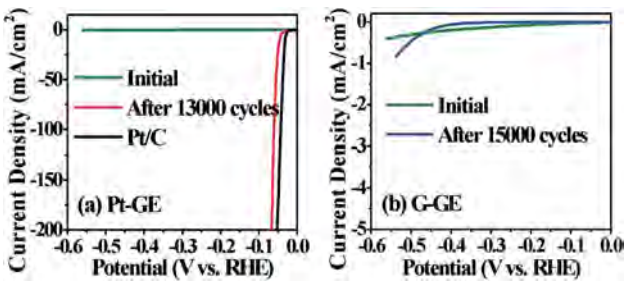

Fig. 1 LSV curves on HER of graphite rods activated with different counter electrodes: (a) curves recorded before and after 13 000 CV cycles activation when using a Pt wire as counter electrode. The black line is the HER curve on commercial Pt/C for comparison; (b) curves collected before and after the activation of 15 000 CV cycles when a graphite rod is used as counter electrode.

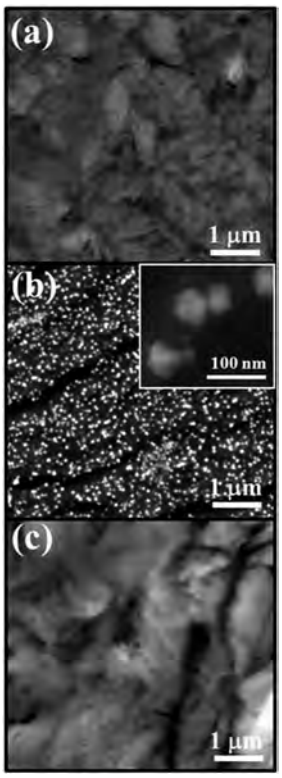

Fig. 2 SEM images of (a) the initial graphite electrode surface, (b) the graphite electrode surface after 13 000 CV activation cycles using a Pt wire as the counter electrode and (c) the graphite electrode surface after 15 000 CV activation cycles with a graphite rod used as the counter electrode. The inset in (b) is the magnified image of the Pt nanoparticles.

eyes. However, after 13 000 CV activation cycles, many tiny and shiny particles could be observed in Fig. 2b, densely dispersed on the surface of Pt-GE when using a Pt wire as the counter electrode. The magnified SEM and TEM pictures (Fig. 2b inset and Fig. 3a and b) further illustrate that the sizes of these particles were less than 100 nm and the shapes of the particles were irregular. Completely different from the surface on the Pt-GE, when a graphite rod was used as the counter electrode, even after 15 000 CV cycles of activation there were no similar particles but only loose graphite layers observed on the surface of G-GE (Fig. 2c). Based on the significant difference in surface morphology and electrochemical properties of Pt-GE and G-GE after different activations, the nanoparticles are thought to be responsible for the greatly elevated HER activity on Pt-GE and the use of the Pt counter electrode must be the decisive factor for the generation of these particles. The elemental analysis of these particles was expected to give further useful information on the mechanism of the electrode activation.

Elemental analysis. The EDS spectra depicted in ESI Fig. S1† show that the commercial Pt wire is highly pure in quality, while ESI Fig. S2† shows that the initial graphite electrode surface mainly consisted of carbon (~96.5 atom%) and oxygen (~3.5 atom%). After the activation of 13 000 CV cycles, the corresponding EDS mapping (Fig. 3) revealed that the elements distributed on the surface of Pt-GE are mostly platinum, carbon and oxygen. A detailed EDS analysis can also be found in ESI Fig. S3.† The signal of S and O can be derived from the absorption of SO_4^{2-} into the background graphite layers of the Pt-GE. All these results clearly suggest that the tiny and shiny nanoparticles are platinum related species on the surface of Pt-GE after the activation.

At the same time, XPS was also employed to study the chemical composition of the electrode surface (Fig. 4). It is clear that when a Pt wire was used as the counter electrode before the activation, only peaks of C 1s and O 1s with binding energies of 284.6 eV and 531.9 eV,[20–22] respectively were observed. After the activation, in addition to C 1s and O 1s peaks, characteristic peaks of Pt $4f_{7/2}$, Pt $4f_{5/2}$, Pt $4d_{5/2}$ and Pt $4d_{3/2}$ were also present at 71.2 eV, 74.4 eV, 314.2 eV and 332.1 eV, respectively.[22–25] Consistent with the previous reports,[23,26,27] if there were oxygen

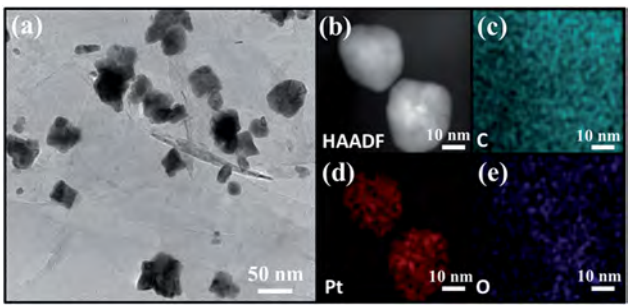

Fig. 3 TEM image (a) and elemental mapping of the graphite electrode surface after an activation of 13 000 CV cycles when using a Pt wire as the counter electrode. (b–e) HAADF-STEM image and corresponding EDS mapping of the Pt particles, indicating the distribution of C, Pt and O, respectively.

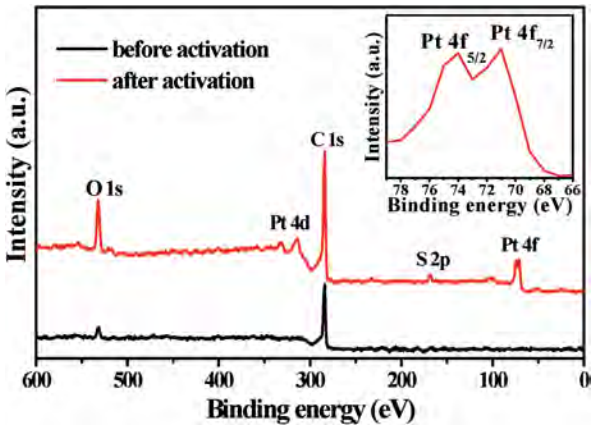

Fig. 4 XPS spectra of the graphite rod before and after an activation of 13 000 CV cycles when using a Pt wire as the counter electrode. The inset gives the detailed characteristics of the Pt 4f spectrum after activation.

atoms absorbed or chemically bonded on the Pt particles, Pt 4f should reveal a shoulder on the high binding energy side of the Pt $4f_{5/2}$ peak at a binding energy of ~76.5 eV; however, there was no such peak in the Pt 4f spectra, indicating that the nanoparticles formed on the surface of Pt-GE are pure metallic Pt particles (Fig. 4 inset). It should also be noted that the weak peak at 169.2 eV can be attributed to S $2p_{3/2}$, which corresponds to the +6 oxidation state of sulfur and demonstrates the existence of SO_4^{2-} in the electrode surface layers. In any case, the XPS results further confirmed the existence of metallic Pt nanoparticles and sulfate ions on the activated electrode surface, which was in accordance with the results from the TEM observation.

3.3 The formation process of Pt particles

Monitoring the activation process as well as understanding the formation process of Pt particles is very important in investigating the transformation process of the working electrode surface during the activation period. Herein, the LSV curves on HER were determined and SEM images were taken as well after different activating CV cycles (ESI Fig. S4 and S5†). As depicted in Fig. S4a,† the onset potential for HER on Pt-GE became smaller with the increasing CV cycles while the corresponding current density went higher and higher at the same time. At the initial 10 000 cycles, the variation of the onset potential and current density was relatively slow. On the other hand, from 10 000 to 12 000 cycles, there was a distinct improvement in the HER activity. These changes are found to have a direct relation to the variation of the electrode surface. ESI Fig. S5† gives the electrode surface evolution of Pt-GE during the activation period. At the beginning, the surface was full of graphite flakes or particles (Fig. S5a and f†). After 4000 CV cycles, some tiny bright nanoparticles began to appear (Fig. S5b and g†). From then till 12 000 CV cycles, more particles were explicitly formed, densely and uniformly dispersed on the electrode surface (Fig. S5c–e and h–j†). Since the highly pure graphite rod (99.999%) was employed as the working electrode during the

activation of Pt-GE, the Pt wire is apparently the only source of Pt and somehow this Pt got transferred from the anode to the cathode, leading to the generation of these Pt nanoparticles, as shown in Fig. 3. In particular, Pt was first dissolved from the wire into the H_2SO_4 solution along with the CV scan. The dissolved Pt species (Pt^{2+} or PtO_x) then dispersed into solution,[28–30] and got reduced to Pt atoms and were regenerated on the cathode surface. The dissolution of Pt is a slow process as the rate determining step; as a result, in the initial thousands of CV cycles, the concentration of Pt species was relatively low and just a few Pt atoms could be regenerated. With the increasing cycles, the concentration of Pt species eventually became higher. According to Le Chatelier's theory, a higher concentration of Pt species would greatly increase the production of Pt atoms on the cathode, and thus more Pt particles would be formed on the cathode surface, which would largely enhance the corresponding electrochemical performance for HER.

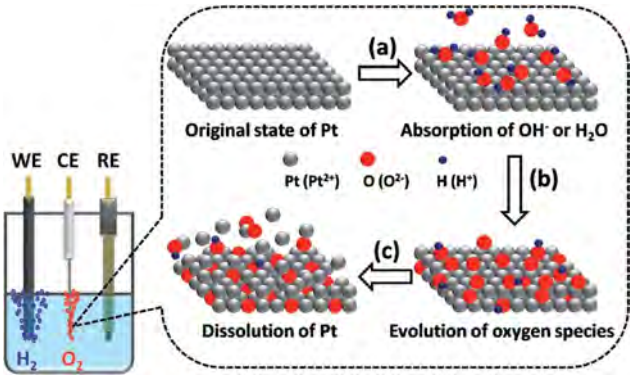

Fig. 5 The possible schematic illustration for the transfer process of Pt from the anode to the cathode. (a) Absorption of OH^- or H_2O on Pt surface, (b) evolution of oxygen species and their reaction with the Pt atoms, (c) position exchange between oxygen and Pt atoms and the dissolution of Pt.

3.4 Possible dissolution mechanism of Pt wire

The dissolution of platinum is an important research topic, which is often studied in the area of polymer electrolyte fuel cells (PEFCs),[30–33] since the dissolution not only washes away Pt from the electrode but also deteriorates the overall performance of PEFCs.[34,35] Many experimental factors, such as temperature, scan rate, as well as variation mode and range of the potential scan, will greatly affect the dissolution rate of Pt.[33,36–40] Matsumoto and Akihiko found that the existence of oxygen can also increase the dissolution rate and the amount of Pt dissolved in acidic environments.[37,39] Although there have been lots of reports on the Pt dissolution, the exact mechanism is still ambiguous. Most researchers have paid much attention to the cathode dissolution of Pt in the high potential range only, which is mainly related to the applications of the oxygen reduction reaction or oxidation of fuels.[29,31,33,35] To the best of our knowledge, there are few reports on the anodic dissolution of Pt in low potential range during the HER process. Based on the previous studies on the dissolution mechanism of Pt,[30,37,39,41] the Pt oxide layer was first formed and then dissolved under the function of the potential scan. During the HER process in low potential range, different oxygen species, such as atomic oxygen (O), peroxide radical ($^{\bullet}HO_2$) and O_2, are generated extensively on the anode,[42] which heavily influences the dissolution progress of Pt. The possible scheme of dissolution of Pt in this study is proposed in Fig. 5. In the first step, H_2O or OH^- is absorbed on Pt surface. Then, these absorbed species are oxidized into the following products: oxygen atoms, $^{\bullet}HO_2$ or O_2 in which the former two are strong oxidizing agents and they would react with Pt instantly after their evolution. In this way, the Pt metal would soon be covered with an oxide layer or become Pt^{2+} ions. Some oxygen atoms may tunnel into the deep layers in this step.[39] In the third step, position exchanges between the Pt atoms and O atoms occur, which would greatly disorder the structure of the surface layers of Pt and weaken the interaction between the surface Pt layer (Pt^{2+} or PtO_x) and the bulk Pt metal, finally leading to the escape of surface Pt species into the solution. These dissolved Pt species then migrate to the cathode area and are regenerated on the Pt-GE by electrochemical or hydrogen reduction. As a result, the Pt-GE is activated gradually and exhibits high catalytic performance on HER.

3.5 Effect of CV cycling on carbon nanohorn catalyst

As discussed in the previous sections, the activation of graphite rod may be ascribed to the deposition of Pt nanoparticles, which were dissolved from the anode. However, the activation behaviour of nano-sized carbon might be different. In this case, carbon nanohorns are a type of carbon nanomaterial with high surface area, good electrical conductivity and close to perfect chemical stability (ESI Fig. S6†). They can be produced in large-scale quantities by DC arc discharge or laser ablation without any metal contamination. CNHs were employed as a substitute for graphite rods and their activation process was studied using the same procedure applied to Pt-GE and G-GE. Similar results to those of graphite rods were acquired and shown in Fig. 6. It is obvious that when a Pt wire was used as the counter electrode, CNHs were effectively activated after 4000 CV cycles; however, when a graphite rod was used as the counter electrode, CNHs were not activated successfully after 4000 CV cycles or even after a potentiostatic treatment of 20 000 s at −2.0 V. All these findings again confirmed that the use of Pt wire is necessary for the successful activation of carbon materials.

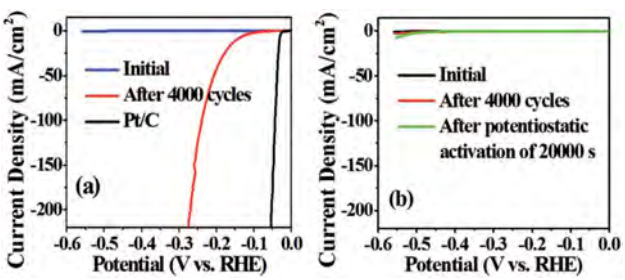

Fig. 6 LSV curves of HER on CNH activated with Pt wire (a) and graphite rod (b) as counter electrodes. The HER curve on commercial Pt/C is also shown for comparison.

4. Conclusions

The activation of graphite rods was investigated using different counter electrodes during the CV cycling process. When a Pt wire was used for activation, the electrochemical catalytic activity of the graphite working electrode was greatly improved to an extent as good as that of commercial Pt/C; however, when a graphite rod was used, the working electrode could not be activated effectively. It was found that the formation of Pt nanoparticles on the cathode surface was the prime reason for the sharp increase in HER catalytic performance under activation with the Pt wire. However, further investigation is needed to determine how the Pt metal gets dissolved in the solution and regenerated onto the cathode for the formation of these Pt nanoparticles. Similar experiments were performed on the carbon nanohorns and consistent results were obtained for the electrochemical catalysis in HER. It can be deduced that the use of Pt wire was essential for the successful activation of carbon materials. In any case, this study suggests that even though platinum is one of the most stable metals and widely used in electrochemical measurement as an inert electrode, its dissolution makes it ineligible for use in strongly acidic and low potential conditions, especially under the continuous CV scan. In some situations, the error caused by Pt dissolution may lead to inaccurate results and wrong conclusions. In order to completely exclude the disturbance from Pt dissolution, an inert counter electrode such as the graphite rod would be an ideal selection.

Acknowledgements

This research was supported by the Early Career Scheme of the Research Grants Council of Hong Kong SAR, China (CityU 139413), the National Natural Science Foundation of China (grant number 51202205) and the Science Technology and Innovation Committee of Shenzhen Municipality (Grant JCYJ-20140419115507588). Moreover, we appreciate Professor Lunhui GUAN from Fujian Institute of Research on the Structure of Matter, Chinese Academy of Sciences, for affording carbon nanohorns.

References

1 J. D. Holladay, J. Hu, D. L. King and Y. Wang, *Catal. Today*, 2009, **139**, 244–260.
2 FuelCellToday, The Industry Review 2013, http://www.fuelcelltoday.com/.
3 A. Ursua, L. M. Gandia and P. Sanchis, *Proc. IEEE*, 2012, **100**, 410–426.
4 R. Subbaraman, D. Tripkovic, K.-C. Chang, D. Strmcnik, A. P. Paulikas, P. Hirunsit, M. Chan, J. Greeley, V. Stamenkovic and N. M. Markovic, *Nat. Mater.*, 2012, **11**, 550–557.
5 C. G. Morales-Guio, L. A. Stern and X. L. Hu, *Chem. Soc. Rev.*, 2014, **43**, 6555–6569.
6 J. Kibsgaard, T. F. Jaramillo and F. Besenbacher, *Nat. Chem.*, 2014, **6**, 248–253.
7 D. S. Kong, H. T. Wang, Z. Y. Lu and Y. Cui, *J. Am. Chem. Soc.*, 2014, **136**, 4897–4900.
8 Z. Zhang, B. P. Lu, J. H. Hao, W. S. Yang and J. L. Tang, *Chem. Commun.*, 2014, **50**, 11554–11557.
9 F. Jiao and H. Frei, *Energy Environ. Sci.*, 2010, **3**, 1018–1027.
10 D. Merki and X. L. Hu, *Energy Environ. Sci.*, 2011, **4**, 3878–3888.
11 J. Q. Zhuo, T. Y. Wang, G. Zhang, L. Liu, L. B. Gan and M. X. Li, *Angew. Chem., Int. Ed.*, 2013, **52**, 10867–10870.
12 W. Cui, Q. Liu, N. Y. Cheng, A. M. Asiri and X. P. Sun, *Chem. Commun.*, 2014, **50**, 9340–9342.
13 R. K. Das, Y. Wang, S. V. Vasilyeva, E. Donoghue, I. Pucher, G. Kamenov, H. P. Cheng and A. G. Rinzler, *ACS Nano*, 2014, **8**, 8447–8456.
14 F. von Sturm, *Angew. Chem.*, 1988, **100**, 1260–1261.
15 W. J. Zhou, Y. C. Zhou, L. J. Yang, J. L. Huang, Y. T. Ke, K. Zhou, L. G. Li and S. W. Chen, *J. Mater. Chem. A*, 2015, **3**, 1915–1919.
16 Y. G. Li, H. L. Wang, L. M. Xie, Y. Y. Liang, G. S. Hong and H. J. Dai, *J. Am. Chem. Soc.*, 2011, **133**, 7296–7299.
17 W. Sheng, Z. Zhuang, M. Gao, J. Zheng, J. G. Chen and Y. Yan, *Nat. Commun.*, 2015, **6**, 5848.
18 S. Iijima, M. Yudasaka, R. Yamada, S. Bandow, K. Suenaga, F. Kokai and K. Takahashi, *Chem. Phys. Lett.*, 1999, **309**, 165–170.
19 N. Li, Z. Y. Wang, K. K. Zhao, Z. J. Shi, Z. N. Gu and S. K. Xu, *Carbon*, 2010, **48**, 1580–1585.
20 L. Shi, R. P. Liang and J. D. Qiu, *J. Mater. Chem.*, 2012, **22**, 17196–17203.
21 A. S. Arico, A. K. Shukla, H. Kim, S. Park, M. Min and V. Antonucci, *Appl. Surf. Sci.*, 2001, **172**, 33–40.
22 J. N. Tiwari, F. M. Pan, R. N. Tiwari and S. K. Nandi, *Chem. Commun.*, 2008, 6516–6518, DOI: 10.1039/b813935k.
23 M. Hiramatsu and M. Hori, *Materials*, 2010, **3**, 1559–1572.
24 M. Li, X. J. Bo, Z. C. Mu, Y. F. Zhang and L. P. Guo, *Sens. Actuators, B*, 2014, **192**, 261–268.
25 M. H. Huang, G. F. Dong, N. Wang, J. X. Xu and L. H. Guan, *Energy Environ. Sci.*, 2011, **4**, 4513–4516.
26 J. S. Hammond and N. Winograd, *J. Electroanal. Chem.*, 1977, **78**, 55–69.
27 C. R. Parkinson, M. Walker and C. F. McConville, *Surf. Sci.*, 2003, **545**, 19–33.
28 K. I. Ota, S. Nishigori and N. Kamiya, *J. Electroanal. Chem.*, 1988, **257**, 205–215.
29 G. Inzelt, B. B. Berkes and A. Kriston, *Pure Appl. Chem.*, 2011, **83**, 269–279.
30 B. E. Conway, *Prog. Surf. Sci.*, 1995, **49**, 331–452.
31 H. S. Liu, C. J. Song, L. Zhang, J. J. Zhang, H. J. Wang and D. P. Wilkinson, *J. Power Sources*, 2006, **155**, 95–110.
32 A. A. Topalov, I. Katsounaros, M. Auinger, S. Cherevko, J. C. Meier, S. O. Klemm and K. J. J. Mayrhofer, *Angew. Chem., Int. Ed.*, 2012, **51**, 12613–12615.
33 L. Kim, C. G. Chung, Y. W. Sung and J. S. Chung, *J. Power Sources*, 2008, **183**, 524–532.
34 S. Shrestha, Y. Liu and W. E. Mustain, *Catal. Rev.*, 2011, **53**, 256–336.

35 R. Borup, J. Meyers, B. Pivovar, Y. S. Kim, R. Mukundan, N. Garland, D. Myers, M. Wilson, F. Garzon, D. Wood, P. Zelenay, K. More, K. Stroh, T. Zawodzinski, J. Boncella, J. E. McGrath, M. Inaba, K. Miyatake, M. Hori, K. Ota, Z. Ogumi, S. Miyata, A. Nishikata, Z. Siroma, Y. Uchimoto, K. Yasuda, K. I. Kimijima and N. Iwashita, *Chem. Rev.*, 2007, **107**, 3904–3951.
36 S. Mitsushima, S. Kawahara, K. I. Ota and N. Kamiya, *J. Electrochem. Soc.*, 2007, **154**, B153–B158.
37 A. Kawano and S. Imabayashi, *J. Electrochem. Soc.*, 2014, **161**, F67–F71.
38 S. Cherevko, A. A. Topalov, A. R. Zeradjanin, G. P. Keeley and K. J. J. Mayrhofer, *Electrocatalysis*, 2014, **5**, 235–240.
39 M. Matsumoto, T. Miyazaki and H. Imai, *J. Phys. Chem. C*, 2011, **115**, 11163–11169.
40 X. P. Wang, R. Kumar and D. J. Myers, *Electrochem. Solid-State Lett.*, 2006, **9**, A225–A227.
41 Y. Sugawara, T. Okayasu, A. P. Yadav, A. Nishikata and T. Tsuru, *J. Electrochem. Soc.*, 2012, **159**, F779–F786.
42 H. Dau, C. Limberg, T. Reier, M. Risch, S. Roggan and P. Strasser, *ChemCatChem*, 2010, **2**, 724–761.

